Ad Hoc Networks 22 (2014) 27–42

Contents lists available at ScienceDirect

Ad Hoc Networks

journal homepage: www.elsevier.com/locate/adhoc

The impact of scalable routing on lifetime of smart grid communication networks

Erkam Uzun [a], Bulent Tavli [a,*], Kemal Bicakci [a], Davut Incebacak [b]

[a] TOBB University of Economics and Technology, Ankara, Turkey
[b] Middle East Technical University, Ankara, Turkey

ARTICLE INFO

Article history:
Received 22 October 2013
Received in revised form 8 April 2014
Accepted 13 May 2014
Available online 20 May 2014

Keywords:
Smart grid
Localized routing
Scalability
Wireless sensor networks
Network lifetime optimization
Mixed integer programming

ABSTRACT

The paradigm of sensors organized in a multi-hop wireless network has been recognized as a cost effective way to satisfy the real-time sensing and communication needs of a smart grid. For wireless sensor networks, one of the most important design goals is the maximization of network lifetime. Scalability, on the other hand, is also of utmost importance for any given network design problem and especially in a wide area smart grid deployment scenario. Improving scalability requires the network flows to be more localized, however, localizing network operations works against the utilization of some optimal paths required for load balancing and lifetime prolonging. Therefore, lifetime maximization and scalability are two design criteria acting against each other. In this study, a characterization of achievable network lifetime as a function of level of localization of the routing operations under optimal conditions is performed using three localized routing approaches. We build a novel Mixed Integer Programming (MIP) framework with a special emphasis on the details of energy dissipation terms in sensor nodes to model the network behavior correctly. Numerical analysis performed using the developed MIP framework enables us to quantify the impact of different levels of route localization on network lifetime.

1. Introduction

The condition of traditional power grids has been started to be questioned after major blackout events affected around 60 million people in Northeast of the United States and Canada on 14th August 2003 and in Italy and Switzerland on 28th September 2003 [1,2]. These incidents unveiled the deficiency in communication, automation, monitoring, and diagnostic tools which failed in determining and evaluating the condition of the power system and had delay in recovery even after a single outage [3–5]. After discovering the need to improve the traditional power systems, institutes such as U.S. Department of Energy (DoE), European Technology Platform (ETP), and Electric Power Research Institute (EPRI) established their smart grid programs for the years 2020 and beyond [6–8]. The vision of smart grid programs is resilience and energy efficiency, future system adaptation, self-healing and automation, and reduction of carbon emissions in power grids. To achieve these goals, the next generation power grids have to incorporate various smart grid applications such as distributed renewable energy generation, distributed storage, sophisticated energy management in consumer side, and intelligent and interactive consumer applications which need improved monitoring, analysis, and control functions [3,4,9,10].

The heart of the smart grid revolution is the ability to monitor the status of the electric grid in a more accurate and fine-grained way. Hence, the real-time communication

* Corresponding author. Tel.: +90 312 292 4074.
E-mail addresses: euzun@etu.edu.tr (E. Uzun), btavli@etu.edu.tr (B. Tavli), bicakci@etu.edu.tr (K. Bicakci), idavut@metu.edu.tr (D. Incebacak).

http://dx.doi.org/10.1016/j.adhoc.2014.05.009
1570-8705/

system is the main part of the smart grid vision. This system could be implemented using various communication technologies including wired, wireless, and power line communication. In the traditional power grid, monitoring and diagnostic systems are realized through wired communications. However, wireline communication systems require high cabling costs in installation and maintenance especially due to the wide geographical spread of the utility assets [11]. For instance, to monitor a typical utility comprised of 25,000 km of power lines and thousands of transformers, capacitors and breakers spread over an 80,000 km^2 area requires over 100,000 distributed sensors and sources of data [12]. Thus, a wireless ad hoc networking approach could be a preferable solution due to low installment and operation costs. It was stated that most utility and billing companies have also recognized that wireless communication becomes one of the most cost-efficient way to collect utility meter data with the invention of low-cost low-power radio sensors [11].

Cost may not be the only differentiator. Available wireless sensor technologies (such as Mica2 motes from Crossbow [12]) could play a significant role in smart grid [13,14] also due to other advantages such as high fault-tolerance, scalability, high sensing fidelity, improved accuracy and larger coverage. As a matter of fact, applications based on Wireless Sensor Networks (WSNs) such as wireless smart meter, deployment of ultra low-power wireless sensor nodes to measure power consumption of residential consumers, remote monitoring and wireless automated meter reading have been started to be implemented by various utility industries in USA and Japan. In addition, numerous WSN applications have increasingly been implemented in transmission and distribution side (T&D) and generation side of smart grids. In Table 1, a categorization of WSN based applications in smart grids is presented [14]. A study by DoE indicates that deployment of WSNs in the industry could improve the production efficiency by 11–18% while reducing the industrial emissions by more than 25% [15].

Table 1
WSNs based smart grid applications [14].

Smart grid side	Application
Consumer side	Wireless automatic meter reading Residential energy reading Automated panels management Building automation Demand-side load management Process control monitoring Properties control monitoring Equipment management and control monitoring
T&D side	Equipment fault diagnostics Overhead transmission line monitoring Outage detection Underground cable system monitoring Conductor temperature rating systems Overhead and underground fault circuit indicators Cable, conductor and lattice theft Conductor temperature and low-hanging conductors Insulators Fault detection and location Animals and vegetation control
Generation side	Real-time generation monitoring Remote monitoring of wind farms Remote monitoring of solar farms Power quality monitoring Distributed generation

For implementing wide-area smart grid systems, a multi-hop network architecture is essential. The sensors collect the data such as meter readings or failure information and send it to a base station possibly via other sensor nodes acting as relays. The base station has a gateway functionality and is controlled by the grid operator.

There are multiple challenges for a successful deployment of wireless sensor networks in smart grids. Power management, interoperability, security, scalability, resource constraints, reliability and latency requirements, and harsh environmental conditions are just some of these challenges [11,14]. These challenges are either due to the nature of WSNs or arise from the harsh environment of smart grids. We note that in some of the applications mentioned in Table 1 (*e.g.*, the monitoring of transmission lines via sensors) the network is not restricted with energy since the energy can be fed from the transmission lines easily. On the other hand, in other applications, due to physical limitations, feeding energy from transmission lines is not an option and it is difficult to charge or replace the battery of a wireless sensor node (for instance when the node is deployed on a monitored device such as solar panel, wind tribune or substation). Hence, energy-efficient networking protocols must be utilized for maximization of the network lifetime.

In multi-hop wireless networks, one important design issue is routing; how to select the path to send the data to the destination. In the literature, there are many routing protocols designed for Wireless Sensor Networks (WSNs). These protocols could be analyzed and compared using various performance metrics. In our vision, we consider scalability as one of the most important metrics for evaluating routing protocols in WSNs deployed in large-scale smart grid applications. In this context, scalability could be defined with respect to network size (*i.e.*, the ability to accommodate the growth in the number of nodes deployed in the network).

When we look at traditional large networks (*e.g.*, Internet), we see that scalability of routing is mainly achieved by dividing a routing domain into several routing areas (autonomous systems) [16]. Different routing protocols are used within and between autonomous systems, complementing each other for end-to-end packet delivery. To put it in more precise terms, an intra-autonomous system routing protocol is used first to bring the data packets to a special gateway router which then runs an inter-autonomous protocol. Finally, another – possibly different – intra-autonomous routing protocol is used to reach the ultimate destination. With this hierarchy, routers need to keep only partial information about the Internet topology (with less memory and processing overhead). Consequently, a more scalable and efficient operation could be achieved.

One distinguishing feature of WSNs is the many-to-one traffic pattern (*i.e.*, rather than a peer-to-peer communication paradigm, the base station is the sink of all data traffic). Hence, a good option to apply the idea of autonomous systems is to make the base station a member

of each system (for instance with pie shaped areas in a disc shaped network topology). By this way, speaking with Internet terminology, no inter-autonomous routing is needed since all data could reach the base station without leaving its autonomous system. Moreover, this is a more resilient architecture because a failure in monitoring the whole power grid is avoided when a single part of the smart grid excluding the base station breaks down by environmental conditions or sabotages.[1] However, as we will see, this simple strategy should be evaluated with respect to one other important performance metric: the impact on network lifetime.

As we have mentioned, network lifetime is an important performance metric in WSNs deployed for smart grids because of finite and unreplenishable battery energy of sensor nodes. If sensor nodes dissipate their energies in a balanced fashion so that over-utilization of energy by any node is avoided, then, according to a common definition, the lifetime of a WSN is maximized. Such collaborative networking approach is shown to outperform greedy solutions which utilizes network resources suboptimally [17]. However, the extent of the collaboration among the nodes is also an important aspect. Intuitively, collaboration of all sensor nodes without any restriction results in maximal network lifetime, however, such global collaboration is not in line with the idea of scalable operation as discussed earlier. Maximization of lifetime and scalability which are among the most important design goals in WSNs [18], are generally acting against each other. There is a conceptual trade-off between maximization of lifetime and scalability in WSNs.

Our purpose in this study is to investigate systematically the trade-off between lifetime maximization and routing scalability through localization in smart grid communication networks. We build a novel Mixed Integer Programming (MIP) framework to investigate the problem under ideal conditions. We do not consider a specific routing protocol in our work. Designing a routing protocol is not our goal, either. Instead, we present a general framework to characterize the performance bounds of localized routing with respect to the impact on network lifetime. We model three localized routing regimes through the proposed framework and analyze the effects on network lifetime.

2. The MIP model for global collaboration

In this section we first present a novel MIP model which forms the base for the rest of our formulations. Then, we carefully introduce additional constraints to account for the significant energy dissipation terms. The MIP model presented in this section is for the case of global collaboration. In the next section, we introduce various extensions for modeling different localized routing regimes. Before presenting the MIP model, we provide a brief background on mathematical programming motivating the use of MIP in our work.

[1] In electric-power grid environment, the wireless sensor nodes could be subject to caustic harsh and damaging environments, high humidity levels, vibrations, dirt and dust, electromagnetic fields, RF interference, and even sabotages [5,11].

2.1. Background on MIP

As examples of mathematical programming models, both Linear Programming (LP) and MIP models are used to find the best solution considering a given set of constraints, which characterize the set of legitimate decisions [19]. Alternative decisions are compared based on their objective function values and the one with the best value (could be the smallest or the largest depending on the nature of the function) is selected as the optimal. Although they are used for the same reason, LP and MIP models cannot be used in place of each other in many settings. Hence, they should not be considered as alternatives. Basically, types of decisions to be made determine which type of a mathematical model should be used to model the problem under consideration. Namely, If the type of decisions to be made take integral values, we need to use integer values. For example in our model introduced shortly, f_{ij}^{k} variable indicates the number of data packets generated by node-k and sent over the arc (i, j). As a result, we can say that the type of mathematical model to be used depends on the type of decisions to be made, which leads to an MIP model for our problem.

In our problem, the objective function is to maximize the network lifetime. To maximize the network lifetime, the amount of data packets flowing over each link should be optimized so that over-utilization of any sensor node's energy resource is prevented (*i.e.*, network-wide energy dissipation is balanced). Indeed, energy efficient protocol design in WSNs is generally achieved by establishing a set of rules in the form of an algorithm. However, most of these algorithms are, essentially, heuristic algorithms that perform suboptimally. On the other hand, when the lifetime maximization problem is cast as an MIP model, then the results obtained by solving the MIP model are guaranteed to be optimal solutions.

LP models whose variables take continuous values are relatively easier to solve. This is due to the special geometry of the set of feasible solutions (called the feasible set) of LPs. The vertices of the feasible set are defined by the constraints of the model and it is known that, given a non-empty feasible set, there is always a vertex solution which is optimal. Hence the well-known Simplex Algorithm, which searches the optimal solution among the vertices greedily, is a quite effective solution method for LPs, on the average. Unfortunately, MIP models do not have such a property in general and hence call for more advanced solution algorithms such as branch-and-bound and branch-and-cut. These methods guaranteeing an optimal solution are called exact solution methods. At each step of such algorithms, first the problem without the integrality restrictions on variables (*i.e.*, the LP relaxation) is solved. Then, if an integer variable (*e.g.*, the one which is actually required to be an integer in the original problem) has a fractional value in the current solution, then the problem is divided into two subproblems by setting that variable's value to the nearest integer values. Then, the new problems are solved recursively in the same manner until the optimal solution is found. This basic method can be improved and fastened by incorporating problem specific information in the subproblem creation step.

The literature on mathematical programming based modeling and analysis of WSNs is extensive and has grown

rapidly in recent years. Providing a comprehensive overview of the published research on modeling WSNs through mathematical programming is beyond the scope of our work. We refer interested readers to the recent review papers on this topic [20,21].

2.2. The base MIP model

In our network model, there is a single base station which collects the data from N sensor nodes which are located on monitored devices in a smart grid network. Each sensor node-i reads the same number of data packets (s_i) from the device periodically and can relay the other sensors' data to the base station. Data packets are treated as indivisible data units (*i.e.*, data packets are neither fragmented nor combined with other data packets until they reach the base station). The network topology is represented by a directed graph, $G = (V, A)$, where V is the set of all nodes including the base station as node-1. We also define set W which includes all nodes except node-1 (*i.e.*, $W = V \setminus \{1\}$). $A = \{(i,j) : i \in W,\ j \in V - i\}$ is the ordered set of arcs. Note that the definition of A implies that no node sends data to itself. Data generated at node-k flowing from node-i to node-j is represented as f_{ij}^k.

The optimization problem for maximizing the network lifetime (the product of number of rounds and the round duration) is presented in Fig. 1.

The objective of our problem implies that the lifetime of the network ends when the first node in the network exhausts its energy. To maximize the lifetime, all nodes are forced to dissipate their energies in a balanced fashion (their battery energies are depleted almost simultaneously).

Eq. (1) states that all flows are non-negative. Eq. (2) states that all data originated at node-k is routed out to the rest of the network including the base station. Eq. (3) is used to avoid loop backs to the source node-k (*i.e.*, a source node cannot receive back any data packets it injected into the network). Eq. (4) states that when a node (node-i) is relaying data of another node (node-k) sum of all node-k's data flowing into node-i (either directly from node-k or via other relay nodes) equals to sum of all node-k's data flowing out of node-i (either directly to the base station or to other relay nodes). Note that Eq. (4) must be satisfied at each node for all other nodes except the base station (in total there are $N-2$ constraints to be satisfied at each node excluding node-1). Eq. (5) is used to ensure that all data generated at each source node eventually flows into the base station (node-1). Eq. (6) guarantees that the sink never transmits any data packets to any sensor nodes. Eq. (7) is used to transform the logical flows (f_{ij}^k) into physical flows (g_{ij}). Note that the index-k is not needed for energy or bandwidth constraints, explained next. Therefore, we remove it for clarity.

Maximize $N_{rnd}T_{rnd}$

Subject to:

$$f_{ij}^k \geq 0 \ \forall k \in W \ \forall (i,j) \in A \tag{1}$$

$$\sum_{(k,j)\in A} f_{kj}^k = N_{rnd}s_k \ \forall k \in W \tag{2}$$

$$\sum_{(j,k)\in A} f_{jk}^k = 0 \ \forall k \in W \tag{3}$$

$$\sum_{(i,j)\in A} f_{ij}^k - \sum_{(j,i)\in A} f_{ji}^k = 0 \text{ if } i \neq k,\ \forall k \in W, \forall i \in W \tag{4}$$

$$\sum_{(j,1)\in A} f_{j1}^k = N_{rnd}s_k \ \forall k \in W \tag{5}$$

$$\sum_{(1,j)\in A} f_{1j}^k = 0 \ \forall k \in W \tag{6}$$

$$\sum_{k\in V} f_{ij}^k = g_{ij} \ \forall k \in W \tag{7}$$

Fig. 1. The base MIP model.

2.3. Energy constraints

Eq. (8) states that total energy dissipation at each node is limited by the amount of energy stored in batteries. The terms on the left side of inequality in Eq. (8) refer to data acquisition, transmission, reception, and sleep energy, respectively. Note that the second term of the inequality in Eq. (8) accounts for the energy dissipation of the node that transmits a data packet and receives an ACK packet during a link level handshake, whereas, the third term of the inequality in Eq. (8) accounts for the energy dissipation of the node that receives a data packet and transmits an ACK packet in reply during a link level handshake. Eq. (9) states that each sensor node is assigned equal initial energy at the beginning of the network operation. Below, we explain the energy terms in more detail.

$$N_{rnd}E_{DA} + \sum_{(i,j)\in A} g_{ij}E_{tx,ij}^D + \sum_{(j,i)\in A} g_{ji}E_{rx,ji}^D + P_{slp}(N_{rnd}T_{rnd} - T_{bsy,i}) \leq e_i \ \forall i \in W \tag{8}$$

$$e_i = battery \ \forall i \in W \tag{9}$$

2.3.1. Data acquisition energy

We assume that time is organized into rounds and each round has a duration of $T_{rnd} = 10$ s. At each round every node dissipates a certain amount of energy for data acquisition ($E_{DA} = 600$ μJ) and generates $M_D = 230$ Bytes of processed data to be conveyed to the base station. Energy dissipation for data acquisition is obtained by using the power for running the MCU and the sensor board in active mode ($P_{DA} = 30.0$ mW) [22] and the total data acquisition and processing time ($T_{DA} = 20$ ms). We utilize Mica2 platform energy dissipation characteristics. Mica2 platform consists of an Atmel Atmega128L processor and Chipcon CC1000 radio. Both of them have well-characterized energy dissipation properties.

2.3.2. Transmission energy

In all forms of digital communications, transmitted bits are received erroneously with a certain probability. The rate of receiving erroneous bits is characterized by the

Bit Error Rate (BER) metric. With the assumption of statistical independence, data packets consisting of bits have also a certain error probability. If a packet is received with errors then the transmitter transmits the same packet again. This operation is known as retransmission.

In our system model, each data packet is assumed to be received successfully with probability $p_{D,s}$ and data packet error rate is $p_{D,f} = 1 - p_{D,s}$. By the same token acknowledgment packets, which are $M_A = 20$ Bytes, have a certain success probability ($p_{A,s}$) and a certain failure probability ($p_{A,f} = 1 - p_{A,s}$). For a given bit error rate ($p_{BER} = 10^{-4}$) packet success probability of an M Byte packet is $(1 - p_{BER})^{8M}$ if there is no forward error correction, which is the case for Mica2 motes.

Each data packet has $M_H = 25$ Bytes of overhead, thus, the data packet length is $M_P = M_H + M_D = 255$ Bytes. Data transmission between a transmitter and receiver pair takes place at a single time slot which has a predetermined time. Perfect synchronization between any transmitter/receiver pair is not achievable, thus, in practical protocol implementations guard times are used at the start and end of a data slot [23]. There are many synchronization protocols designed specifically for WSNs with virtually no overhead and satisfactory synchronization performance [24]. For example, Timing-sync protocol uses piggybacking for synchronization [25], which is reported to have an average synchronization error of 16.9 μs and a worst case error of 44 μs. We assume that such a synchronization scheme is in effect in our system model and all nodes are roughly time-synchronized which enables the correct timing for data transmissions and receptions, especially, when relaying is performed. We choose the guard time to be $T_{grd} = 100$ μs, which is roughly twice the maximum synchronization error.

The time interval between the completion of the data packet transmission at the source node and the beginning of the acknowledgment packet receipt which includes various delay terms (*e.g.*, propagation delay) is modeled by T_{rsp} 500 μs. To account for all of the aforementioned terms the slot time is found as $T_{slot} = \lceil 2 \times T_{grd} + T_{tx}(M_P) + T_{rsp} + T_{tx}(M_A) \rceil = 58$ ms, where $T_{tx}(M_P)$ and $T_{tx}(M_A)$ are the durations of data and acknowledgment packets which are obtained by dividing the number of bits to the channel bandwidth ($\xi = 38.4$ Kbps) [26].

The distance between a transmitter and a receiver cannot be measured with perfect accuracy, however, it is possible to estimate distances with a certain maximum positioning error. For example, experimental results reported in [27] show that it is possible to perform location estimation using RSSI with less than 2 m positioning errors. Hence, we model the distance estimation errors with parameter $d_{err} = 2$ m. If the actual distance between two nodes is d_{ij} meters then the estimated distance (d_{ij}^e) is confined to the interval $[d_{ij} - d_{err}, d_{ij} + d_{err}]$. To avoid transmission with lower power than the actual required power level due to estimation errors, we use the compensated distance $\left(d_{ij}^c\right)$ to transmit packets. Compensated distance is obtained by $d_{ij}^c = d_{ij}^e + d_{err}$.

We use the energy dissipation model for Mica2 motes equipped with CC1000 radios presented in [28]. Transmission ranges and corresponding energy dissipations for this model are presented in Table 2. Power consumption for transmission at power level l is denoted as $P_{tx}(l)$ and the maximum transmission range at power level l is denoted as $R_{max}(l)$. The set of power levels is denoted as S_L. Power consumption for reception is constant and denoted as $P_{rx} = 35.4$ mW. Each node chooses the optimal transmission power dynamically for each flow. The optimal power level to transmit over a distance d_{ij}^c (l_{ij}^{opt}) is given in Eq. (10). Furthermore, Eq. (11) is used to limit the maximum transmission range of each node, where ϱ is the maximum transmission range possible ($\varrho = 82.92$ m). Note that if data packets are not replied with ACK packets consistently then the transmitter will know that the intended recipient is beyond its effective transmission range.

Table 2
Transmission power consumption, $P_{tx}(l)$, in milliWatts and maximum transmission ranges, $R_{max}(l)$, in meters at each power level (l) for the Mica2 motes equipped with CC1000 radios as a function of power level (l) [28].

l	$P_{tx}(l)$	$R_{max}(l)$	l	$P_{tx}(l)$	$R_{max}(l)$
1	25.8	19.30	14	32.4	41.19
2	26.4	20.46	15	33.3	43.67
3	27.0	21.69	16	41.4	46.29
4	27.1	22.69	17	43.5	49.07
5	27.3	24.38	18	43.6	52.01
6	27.8	25.84	19	45.3	55.13
7	27.9	27.39	20	47.4	58.44
8	28.5	29.03	21	50.4	61.95
9	29.1	30.78	22	51.6	65.67
10	29.7	32.62	23	55.5	69.61
11	30.3	34.58	24	57.6	73.79
12	31.2	36.66	25	63.9	78.22
13	31.8	38.86	26	76.2	82.92

$$l_{ij}^{opt} = \underset{l \in S_L, d_{ij}^c \leqslant R_{max}(l)}{\operatorname{argmin}} \left(E_{tx}(l)\right) \tag{10}$$

$$g_{ij} = 0 \text{ if } d_{ij}^c > \varrho \ \forall (i,j) \in A \tag{11}$$

Energy dissipation for transmitting M_P Bytes of data from node-i to node-j is given in Eq. (12).

$$E_{tx,ij}^{P}(M_P) = P_{tx}\left(l_{ij}^{opt}\right) T_{tx}(M_P) \tag{12}$$

A transmitting node stays in the receive mode except the time it transmits the data packet. Note that in CC1000 radios there is no difference in energy dissipation for actual data reception or idle listening. The total energy dissipation of a transmitter in a slot (during a single handshake) is given in Eq. (13).

$$E_{tx,ij}^{HS}(M_P, M_A) = E_{tx,ij}^{P}(M_P) + P_{rx}(T_{slot} - T_{tx}(M_P)) \tag{13}$$

Even if the transmitted data packet cannot be received by the destination due to bit errors the amount of energy dissipated by the transmitter is the same because the transmitter has to listen to the acknowledgment packet. The lack of an acknowledgment packet in response to the data packet transmission indicates a packet loss. The probability of a successful handshake is $p(HS,s) = p_{D,s}p_{A,s}$ and the probability of a failed handshake is $p(HS,f) = 1 - p(HS,s)$. On the average, each data packet has to be transmitted $1/p(HS,s)$ times.

Finally, the transmitter's energy dissipation value including the effects of packet failures and packet process-

ing energy dissipation is presented in Eq. (14) (packet processing energy is dissipated only once and subsequent retransmissions do not incur additional packet processing energy dissipation). Each node dissipates $E_{PP} = 120\ \mu J$ amount of energy for packet processing. Packet processing energy is obtained by using the power consumption of Mica2 platform in MCU active mode (24.0 mW) [29] and the total utilization time of the CPU for each packet.

$$E^{D}_{tx,ij} = \frac{1}{p(HS,s)} E^{HS}_{tx,ij}(M_P, M_A) + E_{PP} \tag{14}$$

2.3.3. Reception energy

Energy dissipation for receiving a data packet and replying with an acknowledgment packet without any packet error is given in Eq. (15). The handshake can be failed due to bit errors in the acknowledgment packet, however, such a failure has the same energy cost on the receiver's side. If the handshake failure is because of the bit errors in the received data packet then the energy cost of it is given in Eq. (16). Since the data packet is not successfully received, the receiving node switches to the sleep mode upon expiration of the maximum amount of time to receive a data packet. Receiver's energy dissipation including the effects of packet failures is presented in Eq. (17).

$$E^{HS,s}_{rx,ji}(M_P, M_A) = P_{rx}(T_{slot} - T_{tx}(M_A)) + E^{p}_{tx,ij}(M_A) \tag{15}$$

$$E^{HS,f}_{rx,ji}(M_P) = P_{rx} T_{slot} \tag{16}$$

$$E^{D}_{rx,ji} = \left\{ \begin{array}{l} E^{HS,s}_{rx,ji}(M_P, M_A) + E_{PP} + \\ \frac{1}{p(HS,s)} \left[\begin{array}{l} p_{D,s} p_{A,f} E^{HS,s}_{rx,ji}(M_P, M_A) \\ + p_{D,f} E^{HS,f}_{rx,ji}(M_P) \end{array} \right] \end{array} \right\} \tag{17}$$

2.3.4. Sleep energy

If a node is not a receiver or a transmitter at any slot or if it is not acquiring data then it is in the sleep mode. Hence the total sleep time can be obtained from the total busy time which is calculated as in Eq. (18). Note that we assume that packet processing is performed during the active slots.

$$T_{bsy,i} = \frac{T_{slot}}{p(HS,s)} \left[\sum_{(i,j)\in A} g_{ij} + \sum_{(j,i)\in A} g_{ji} \right] + N_{rnd} T_{DA} \tag{18}$$

2.4. Bandwidth constraints

In a broadcast medium, we need to make sure that the bandwidth required to transmit and receive at each node is lower than or equal to the total bandwidth. Such a constraint should take the shared capacity into consideration. We refer to the flows around node-i which are not flowing into or flowing out of node-i and affect the available bandwidth to node-i as interfering flows. Eq. (19) presents the constraint for bandwidth. For all nodes including the base station the aggregate duration of incoming flows, outgoing flows, and interfering flows is upper bounded by the total network lifetime. Note that for sensor nodes (not for the base station) data acquisition time ($N_{rnd}T_{DA}$) is added to the left side of the Eq. (19). This constraint is a modified version of the sufficient condition given in [30,31].

$$\frac{T_{slot}}{p(HS,s)} \left[\sum_{(i,j)\in A} g_{ij} + \sum_{(j,i)\in A} g_{ji} + \sum_{(j,k)\in A} g_{jk} I^{i}_{jk} \right] \leqslant N_{rnd} T_{rnd} \ \forall i \in V \tag{19}$$

Interference function $\left(I^{i}_{jk}\right)$ is formulated in Eq. (20). If node-i is in the interference region of the transmission from node-j to node-k, then the value of interference function for node-i (I^{i}_{jl}) is unity, otherwise it is zero. Generally speaking, interference range is equal to or greater than transmission range (*i.e.*, $\gamma \geqslant 1$). This means depending on the value of γ ($\gamma = 1.7$ is used in this study), node-j's transmission to node-k can interfere with node-i even if the distance between node-j and node-k is less than the distance between node-j and node-i.

$$I^{i}_{jk} = \left\{ \begin{array}{ll} 1 & \text{if } \gamma R_{max}\left(I^{opt}_{jk}\right) \geqslant d_{ji} \text{ and } i \neq j \\ 0 & \text{else} \end{array} \right. \tag{20}$$

In summary, we utilize the interference function to determine whether a flow creates any interference at any other node by using Eq. (20). In fact, this equation determines the flows that can concurrently coexist without creating any interference to each other. Interference range is the key factor in determining the interference of one flow to another, which is a well known abstraction for wireless networks. Therefore, packet errors occur due to noise but not the interference from the other nodes' transmissions provided that Eq. (19) is in effect. Eq. (19) is used to guarantee that the flows in the network can be scheduled within the given time and bandwidth. For example, if we reduce the bandwidth from 38.4 Kbps to 4 Kbps then we would not obtain any feasible solution of the MIP problem which means that it is not possible to come up with any schedule under the given constraints. All system variables with their acronyms and descriptions are presented in Table 3.

3. Extensions for localized routing regimes

In the subsequent subsections, extensions of the model introduced in previous section are presented for modeling three localized routing regimes which organize the sensor nodes in smart grid network by forming groups or domains.

3.1. Per group routing regime

In Per Group Routing Regime (PGRR), the smart grid network is partitioned into non-overlapping domains $\left(D^{PGRR}_{q}\right)$ and the union of all domains constitutes the network (D^{PGRR}_{net}). In fact, this scheme is inspired by dividing a routing domain into several routing areas in the Internet for scalability [16]. In PGRR, inter-domain data transfer is not allowed for improved scalability (*i.e.*, each domain is isolated so that adding new domains do not increase the complexity of routing operations). Therefore, each domain must be self sufficient (*i.e.*, data collected in each domain

Table 3
Terminology, nomenclature, variables, parameters.

Acronym	Description/value	Acronym	Description/value
N	Number of nodes	ξ	Bandwidth (38.4 Kbps)
N_{rnd}	Number of rounds network survives	$T_{tx}(M)$	Time to transmit an M-Byte data packet(s)
f_{ij}^{k}	Total number of data packets generated at node-k and transmitted from node-i to node-j	T_{slot}	Slot duration (58.0 ms)
g_{ij}	Total number of data packets transmitted from node-i to node-j	d_{ij}	Actual distance between node-i and node-j (m)
$G=(V,A)$	Directed graph that represents network topology	d_{err}	Maximum distance estimation error (2 m)
V	Set of nodes, including the base station as node-1	d_{ij}^{e}	Estimated distance of node-i and node-j (m)
W	Set of nodes, except the base station (node-1)	d_{ij}^{c}	Compensated distance of node-i and node-j (m)
A	Set of edges	S_L	The set of power levels
s_i	Number of data packets gathered at node-i from monitored device at each round	l_{jk}^{opt}	Optimal power level between node-j and node-k
E_{PP}	Packet processing energy dissipation (120 μJ)	$P_{tx}(l)$	Power consumption for transmission at power level l (W)
P_{DA}	Data acquisition power consumption (30.0 mW)	P_{rx}	Power consumption for reception (35.4 mW)
T_{DA}	Data acquisition time at each round (20 ms)	P_{slp}	Power consumption in the sleep mode (0.03 mW)
E_{DA}	Data acquisition energy dissipation at each round (600 μJ)	$R_{max}(l)$	Maximum transmission range at power level l (m)
e_i	Battery energy of node-i (J/W h)	ϱ	Maximum transmission range possible (82.92 m)
battery	Initial energy stored in two AA batteries (25.0 kJ = 6.95 W h)	$E_{tx,ij}^{p}(M)$	Energy for transmitting an M-Byte packet data from node-i to node-j (J/W h)
M_P	Data packet size (255 Bytes)	$E_{tx,ij}^{HS}(M_P,M_A)$	Energy dissipation of a transmitter (node-i) for a successful handshake (J/W h)
M_H	Data packet overhead size including the synchronization information (25 Bytes)	$E_{tx,ij}^{D}$	Energy consumption of a transmitter for a handshake including retransmissions (J/W h)
M_D	Data packet payload size (230 Bytes)	$E_{rx,ji}^{HS,s}(M_P,M_A)$	Energy dissipation of a receiver (node-j) for a successful handshake (J/W h)
M_A	Acknowledgment packet size (20 Bytes)	$E_{rx,ji}^{HS,f}(M_P)$	Energy dissipation of a receiver (node-j) for a failed handshake (J/W h)
p_{BER}	Bit error rate (10^{-4}) [32]	$E_{rx,ji}^{D}$	Energy dissipation of a receiver for a handshake including retransmissions (J/W h)
$p_{D,s}$	Data packet success rate	I_{jl}^{i}	Interference function
$p_{D,f}$	Data packet failure rate	γ	Interference range (1.7)
$p_{A,s}$	Acknowledgment packet success rate	D_q^{PGRR}	Domain-q in PGRR model
$p_{A,f}$	Acknowledgment packet failure rate	θ^{PGRR}	Polar angle in PGRR model (°)
$p(HS,s)$	Handshake packet success rate	D_{net}^{PGRR}	Union of all domains in PGRR model
$p(HS,f)$	Handshake packet failure rate	D_k^{PSRR}	Source node-k's routing domain in PSRR model
T_{rnd}	Duration of one round (10 s)	θ^{PSRR}	Polar angle of source node-k's routing domain in PSRR model (°)
T_{grd}	Guard time (100 μs)	D_i^{PRRR}	Relay node-i's routing domain in PRRR model
$T_{bsy,i}$	Total busy time for node-i (s)	θ^{PRRR}	Polar angle of relay node-i's routing domain in PRRR model (°)
T_{rsp}	Response time (500 μs)	θ^{x}	Central angle for all strategies (°)

should be transferred to the base station without intervention from the nodes of other domains). Therefore, the base station is a member of each domain which is the only node that is a member of multiple groups. Hence, in a disc shaped network topology, pie shaped domains are the logical choice that fulfills aforementioned design criteria. Each pie shaped region's vertex is the base station and the radii of all regions equal to the network radius. Hence, the size of pie shaped regions are characterized only by the polar angle θ^{PGRR}. This constraint is modeled in Eq. (21).

$$f_{ij}^{k}=0 \text{ if } \; i\in D_q^{PGRR} \text{ and } \; j\notin D_q^{PGRR} \quad \forall k\in W\ \forall i\in W\ \forall j\in W\ \forall D_q^{PGRR}\in D_{net}^{PGRR} \tag{21}$$

An example PGRR scenario is illustrated in Fig. 2 with four non-overlapping domains (*i.e.*, with $\theta^{PGRR}=90$) marked as D_1^{PGRR}, D_2^{PGRR}, D_3^{PGRR}, and D_4^{PGRR}. The union of these four domains constitutes the network $\left(D_{net}^{PGRR}=D_1^{PGRR}\cup D_2^{PGRR}\cup D_3^{PGRR}\cup D_4^{PGRR}\right)$. Fig. 2 shows the routing path and flows from a source node (node-1) to the base station (node-0) in D_1^{PGRR}. Source node-1 uses two paths to send its data to the base station. The first path carries 59% of the source node-1's generated data and uses only node-2 as a relay, thus, it is a two hop path. The second path carries 41% of the source node-1's generated data and it is a three hop path which employs node-3 and node-4 as relays. Note that source node-1 is close to the border between D_1^{PGRR} and D_4^{PGRR}. Although node-6 is close to the source node-1, node-6 cannot be used as a relay by source node-1 because they are in different routing domains.

3.2. Per source routing regime

Sensor nodes located closer to the borders of the PGRR domains (*e.g.*, node-1 in Fig. 2) are put in a disadvantageous situation due to the fact that the potential set of relay nodes that can transport data more energy efficiently are not in the same domain with these source nodes. Therefore, we propose Per Source Routing Regime (PSRR),

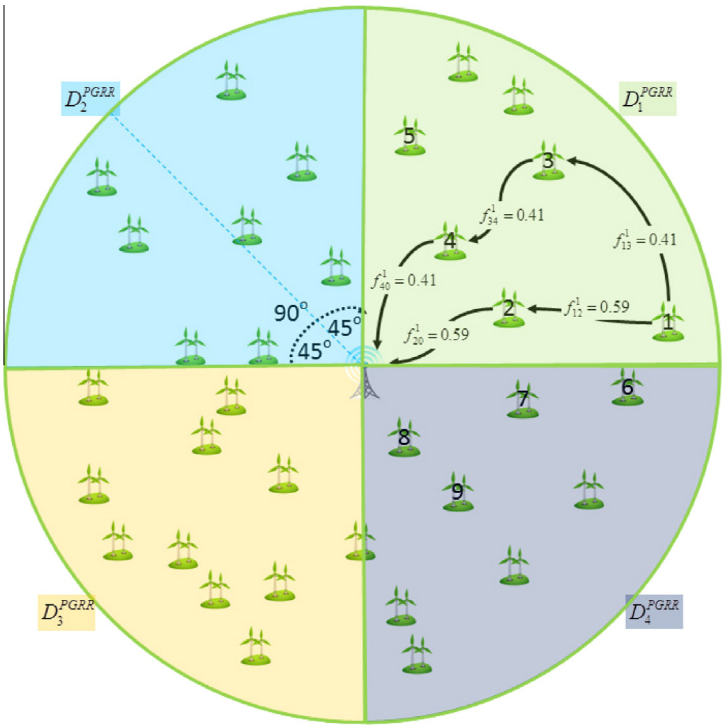

Fig. 2. Illustration of PGRR regime. The channel bandwidth is 38.4 Kbps. The base station is equipped with an Atmega128L processor.

where each source node is on the bisector of its own pie shaped routing domain. All pie shaped regions have their vertices at the center of the deployment area (*i.e.*, the base station is the vertex of all PSRR routing domains). The pie shaped region of source node-k is denoted as D_k^{PSRR} and its polar angle is denoted as θ^{PSRR}. Source node-k's data cannot be forwarded out of region D_k^{PSRR}. This constraint is modeled in Eq. (22).

$$f_{ij}^k = 0 \text{ if } j \notin D_k^{PSRR} \ \forall k \in W \ \forall i \in W \ \forall j \in W \tag{22}$$

An example PSRR scenario is illustrated in Fig. 3 with $\theta^{PSRR} = 90$. In this case, source node-1 is located on the bisector of D_1^{PSRR}. Polar angle θ^{PSRR} determines the extent of the pie shape region. Node-1's data is forwarded by the sensor nodes positioned within the pie shaped PSRR routing domain of node-1.

3.3. Per relay routing regime

Although PSRR mitigates the border effects of PGRR for source nodes, for relay nodes similar disadvantageous situations are not mitigated by the same token (*e.g.*, node-8 in Fig. 3 could be helpful in relaying the data coming from node-7, however, since node-8 is not in D_1^{PSRR}, it cannot forward node-1's data). Thus, in Per Relay Routing Regime (PRRR), not only the source nodes but also the relay nodes have their own routing domains (*i.e.*, each relay node sits on the bisector of its own pie shaped routing domain and the vertex of each pie shaped region is the base station). The pie shaped region of relay node-i is denoted as D_i^{PRRR} and its polar angle is denoted as θ^{PRRR}. Relay node-i cannot forward data out of region D_i^{PRRR}. This constraint is modeled in Eq. (23).

$$f_{ij}^k = 0 \text{ if } j \notin D_i^{PRRR} \ \forall k \in W \ \forall i \in W \ \forall j \in W \tag{23}$$

An example PRRR scenario is illustrated in Fig. 4 with $\theta^{PRRR} = 90$. In this case, not only the source node-1 but also the relay nodes have their own routing domains. For the sake of simplicity, routing domains of only source node-1, relay node-6, and relay node-7 are illustrated in Fig. 4. Note that relay node-8 can be used in PRRR regime which cannot be utilized if the regime were PGRR.

4. Analysis

In this section, we investigate network lifetime achieved by three routing regimes through numerical evaluations of the MIP formulations used to model these regimes. By varying the vertex angle we explore the effects of localized routing on network lifetime. We also investigate the impact of node density by varying the number of nodes in the network while keeping the network area constant.

For this analysis, we consider a WSN deployed on a wind farm [33]. The prediction of wind farm output power is important to increase the wind power capacity and improve the safety and economy of the system. The wind farm output power is related to meteorological data. A WSN could collect and transmit the necessary data such as wind speed and temperature which are used as training and prediction samples of a wind farm output power prediction model stored on a central server [33].

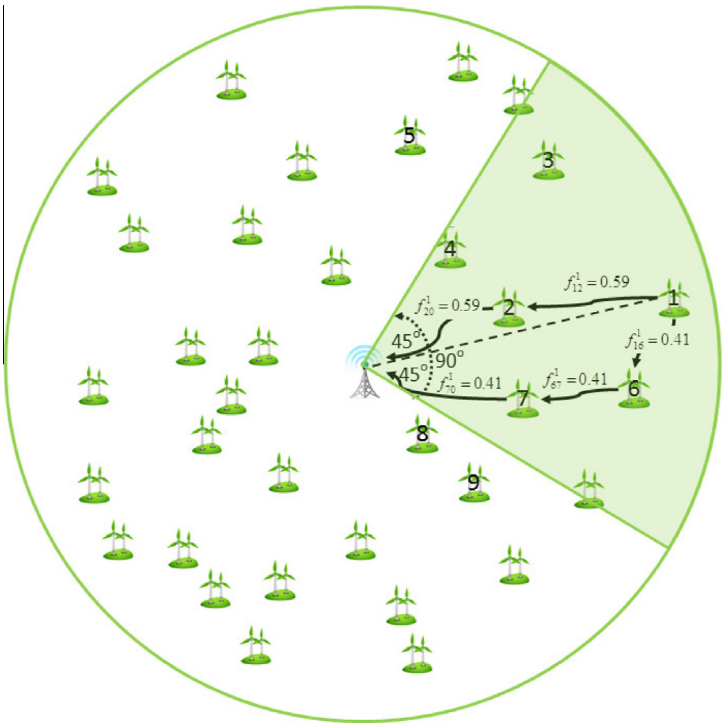

Fig. 3. Illustration of PSRR regime. The channel bandwidth is 38.4 Kbps. The base station is equipped with an Atmega128L processor.

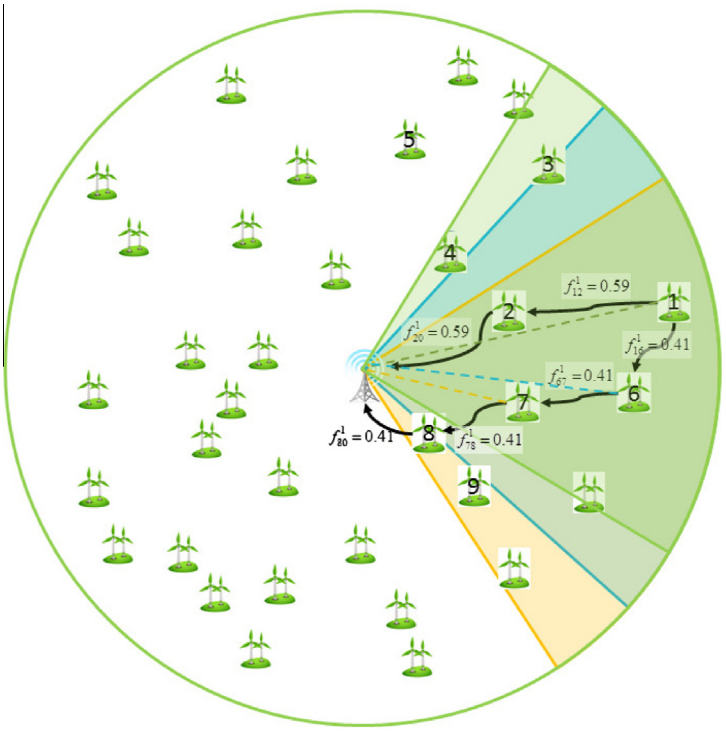

Fig. 4. Illustration of PRRR regime. The channel bandwidth is 38.4 Kbps. The base station is equipped with an Atmega128L processor.

We use General Algebraic Modeling System (GAMS) [34] for the numerical analysis of the developed MIP model. GAMS consists of high-performance solvers for solving MIP models efficiently each of which improves upon the basic approach in different ways to attain an increased solution performance. Hence, when we solve our MIP models using GAMS, one of these solvers is used to obtain the best solution. Specific implementation details are beyond the scope of this paper, however, we present the general approach for solving MIP problems in Section 2.

In our analysis, each sensor node reads one data packet per round ($s_i = 1$) from monitored device. Each node is assumed to be equipped with two AA batteries (*battery* = 25.0 K J = 6.95 W h). We use a disc shaped network topology of radius 100 m. The base station is located at the center of the disc. The distribution of sensors across the network could be an important parameter for route optimization. Without loss of generality, we assume sensor nodes are randomly distributed (uniform distribution) over the network area.

Based on the established theory of optimization, it is evident that localized routing schemes exacerbates the problem of energy over-utilization in a subset of nodes acting as relays and thus have a negative effect on network lifetime. However, we note that the net effect of the localized routing regimes on network lifetime is unclear without the analysis given below.

In Fig. 5, the effects of the level of localization is illustrated by using three selected topologies for a wind farm (two cases presented in each row is obtained by using the same topology). In the upper row of Fig. 5, the paths used by node-2 to route its data towards the base station is presented for $\theta^{PGRR} = 30$ (Fig. 5)) and $\theta^{PGRR} = 60$ (Fig. 5(b)). Note that all sensor nodes read data from wind tribunes and route the its gathered data plus the data coming from other sensors towards the base station, however, presenting all flows would make the figure too complicated, therefore, we present the flows for data generated at node-2 only. Total traffic generated by node-2 is normalized to unity. In PGRR regime, nodes can route data within their domain only, thus, when $\theta^{PGRR} = 30$ (Fig. 5(a)) node-2 transfers all its data directly to the base station. The normalized lifetime (LT) for $\theta^{PGRR} = 30$ is obtained as 0.78. Normalization is achieved by dividing the absolute lifetime obtained by the lifetime obtained with $\theta^{PGRR} = 360$ (*i.e.*, there is no restriction on route selection). Enlarging the routing domain by using $\theta^{PGRR} = 60$ (Fig. 5(a)) results in a prolonged network lifetime (LT = 0.90). For $\theta^{PGRR} = 60$ node-2 routes most of its data via node-4 and node-6 (*i.e.*, only 1.8% of node-2 is transmitted directly to the base station). Although node-2 is closer to the base station than node-6, node-2 sends 47.9% of its data to node-6 because node-2 uses most of its energy to relay the data of node-1, which is the optimal decision for obtaining the maximum network lifetime (*i.e.*, the nodes are not using greedy routing instead they collaborate to prolong the network lifetime).

The middle row of Fig. 5 illustrates the effects of increasing θ^{PSRR} on the flow patterns and network lifetime for node-34. In PSRR regime a source node (node-34 in Fig. 5(c) and (d)) is confined to a pie shaped region centered at the origin to route its data out. When $\theta^{PSRR} = 30$ the normalized lifetime is obtained as 0.81 and source node-34 sends all its gathered data from tribune to node-36 and in turn node-36 relays all of node-34's data to the base station. When $\theta^{PSRR} = 180$ node-34's data is relayed to the base station by collaboration of 6 relay nodes (*i.e.*, node-3, node-4, node-5, node-6, node-7, and node-9). 48.6% of node-34's data is conveyed to the base station by using a four hop path (node-34 → node-7 → node-5 → node-3 → node-0). 48.3% of node-34's data reach the base station via a three hop route (node-34 → node-6 → node-4 → node-0). Node-9 relays 3.1% of node-34's data to the base station (a two hop path). Furthermore, node-36 is not among the relay nodes that transport node-34's data which shows that limiting the routing domain leads to suboptimal relay assignments. It is also interesting to see that collaboration of half of the network is not enough to prevent a 7.0% decrease in network lifetime when compared to the case where the whole network collaborates.

The operation of PRRR regime is illustrated at the bottom row of Fig. 5 for $\theta^{PRRR} = 30$ (Fig. 5)) and $\theta^{PRRR} = 90$ (Fig. 5(f)). Node-5 is the sensor node we investigate in these figures. For $\theta^{PRRR} = 30$ normalized network lifetime is obtained as 0.78. Node-5 routes all its gathered data from the wind tribune to the base station via a two hop path (node-5 → node-7 → node-0). Although node-4 and/or node-6 could relay node-5's data, such data splitting is not the best routing decision that maximizes network lifetime. When $\theta^{PRRR} = 90$ node-5's data is routed to the base station via six relay nodes (node-1, node-2, node-3, node-7, node-34, and node-35). Normalized network lifetime is 0.92 for $\theta^{PRRR} = 90$.

Fig. 5 is illustrative for understanding the tradeoff in limiting the routing domain and prolonging network lifetime. However, we need to explore the parameter space by varying the network size. Furthermore, to obtain statistically meaningful results averages of multiple random topologies need to be taken. In the rest of this section we present analysis for larger topologies.

In Fig. 6(a–c), normalized network lifetime is plotted as a function of θ^{PGRR}, θ^{PSRR}, and θ^{PRRR}, respectively, for $N = 36$, $N = 48$, $N = 60$, and $N = 72$. Normalization is achieved by dividing all network lifetime values by the largest lifetime value which is obtained for $\theta^{PGRR} = \theta^{PSRR} = \theta^{PRRR} = 360$ (*i.e.*, there are no restriction on nodes' collaboration due to separated domains). For all routing regimes network lifetime increases monotonically as the restrictions on the routing areas are relaxed. For example, normalized lifetimes are 0.26 (PGRR), 0.27 (PSRR), and 0.28 (PRRR) for $N = 60$ and $\theta^x = 30$ (θ^x is used to denote the polar angle for all strategies), whereas for $N = 60$ and $\theta^x = 120$ normalized lifetimes are 0.93 (PGRR), 0.94 (PSRR), and 0.95 (PRRR). Normalized lifetime values gets larger as the node density increases due to increase in number of relaying options (*e.g.*, PSRR normalized lifetimes with $\theta^{PSRR} = 60$ are 0.46 and 0.79 for $N = 36$ and $N = 72$, respectively).

Fig. 7 presents the normalized network lifetime as functions of θ^x for different regimes and different node densi-

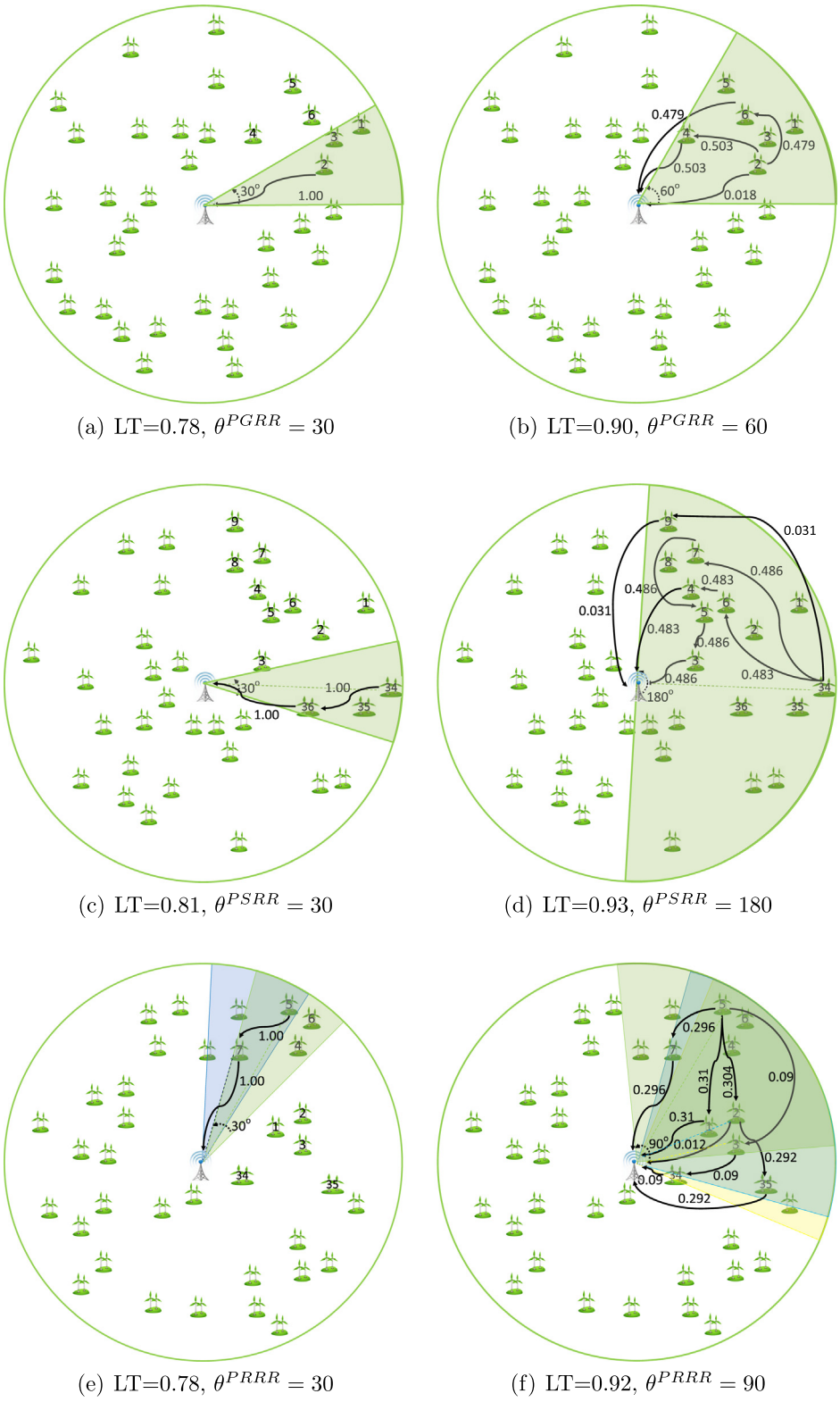

(a) LT=0.78, $\theta^{PGRR} = 30$ (b) LT=0.90, $\theta^{PGRR} = 60$

(c) LT=0.81, $\theta^{PSRR} = 30$ (d) LT=0.93, $\theta^{PSRR} = 180$

(e) LT=0.78, $\theta^{PRRR} = 30$ (f) LT=0.92, $\theta^{PRRR} = 90$

Fig. 5. Illustration of the effects of route localization on network lifetime with $N = 36$ (all angle values are in degrees).

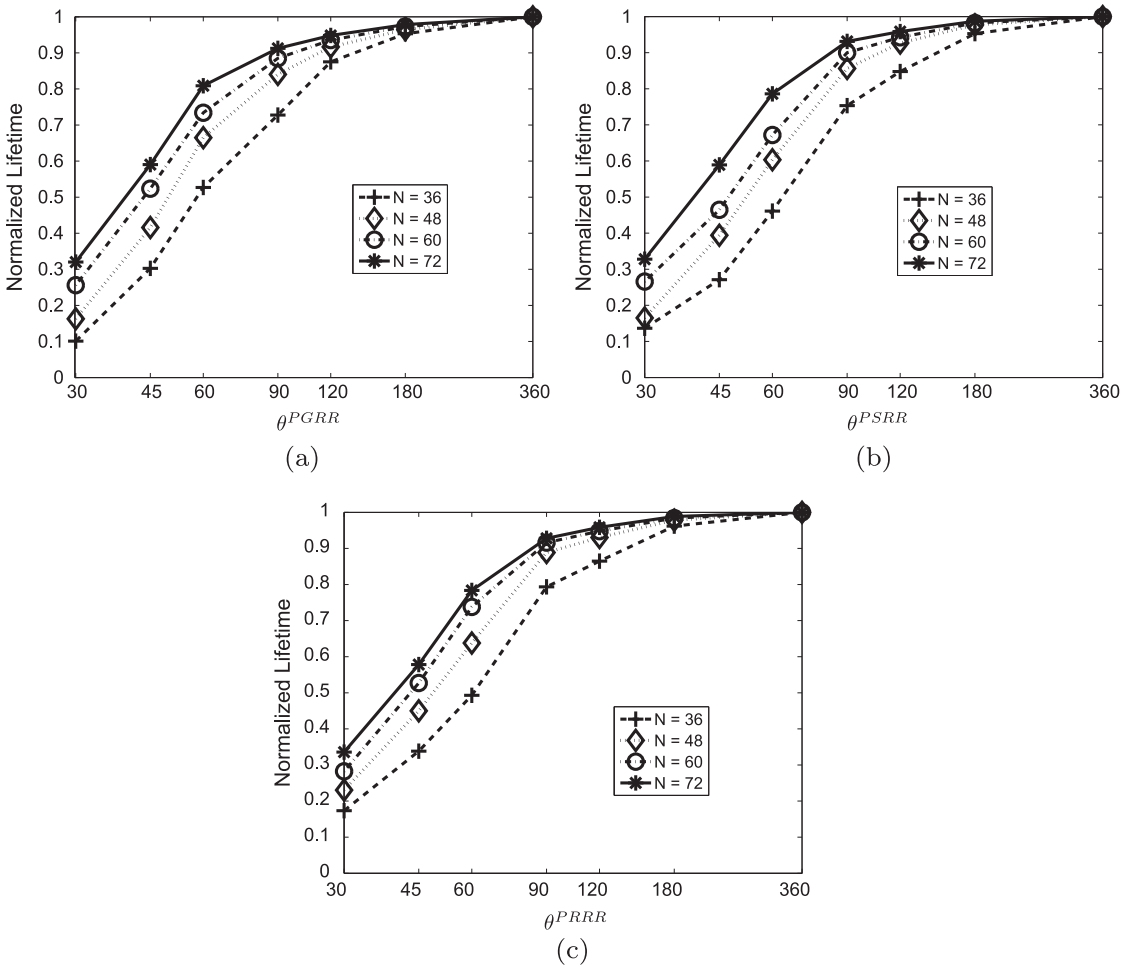

Fig. 6. Normalized lifetime as functions of (a) θ^{PGRR}, (b) θ^{PSRR}, and (c) θ^{PRRR}. Data points presented in the figure are the averages of 500 independent runs.

ties. The main purpose of this figure is to show the lifetime differences obtained with different regimes. In fact, we want see whether relaxing the hard routing domains results in better energy balancing and prolonged network lifetime. When the three regimes are compared, the general trend is that PRRR lifetimes are larger than PSRR lifetimes which in turn is larger than PGRR lifetimes for the same parameter set. The differences in lifetimes are larger especially in more restricted routing domains and sparser networks. For example, with $\theta^x = 30$ and $N = 36$ the normalized network lifetimes of PGRR, PSRR, and PRRR are 0.10, 0.13, and 0.17, respectively. On the other hand, for $\theta^x = 120$ and $N = 60$ the normalized network lifetimes of PGRR, PSRR, and PRRR are 0.93, 0.94, and 0.95, respectively. Nevertheless, the extent of the difference is not significant (*i.e.*, less than 2% difference, on the average).

Fig. 8 presents detailed energy dissipation terms for various θ^x and N values. Energy dissipation values are given in terms of per node per round. The decomposition of energy dissipation is according to the order given in Eq. (8) (data acquisition, transmission, reception, and sleep). The dominant term is the transmission energy dissipation. Data acquisition energy dissipation is constant. Although sleep energy dissipation shows slight variations, the change in sleep energy dissipation is negligibly low. Both transmission and reception energy dissipations decrease as θ^x increases for all three regimes because as the routing domain expands, more energy efficient routing paths arise. Total energy dissipations of all three regimes are within 1% neighborhood of each other for θ^{180}.

Both the number of constraints and the number variables affect time complexity of the MIP solutions. The variables are the flows $\left(f_{ij}^k\right)$, thus, the size of the parameter space is N^3, hence, we expect the solution times to increase exponentially with increasing N. However, the complexity of two problems having the same N can vary significantly depending on the network topology (*i.e.*, convergence time of the MIP solvers strongly dependent on the specific problem instance). Furthermore, different constraints associated with each routing regime also affect the solution times. In Table 4, computation times of the MIP models for three routing regimes are presented. Solution times increase exponentially along each row with increasing N. For example, solution times for $\theta^{PRRR} = 45$ are 1.34 ± 0.14 s and 10.04 ± 1.00 s for $N = 36$ and $N = 72$. Also, for each regime, solution times increase along the

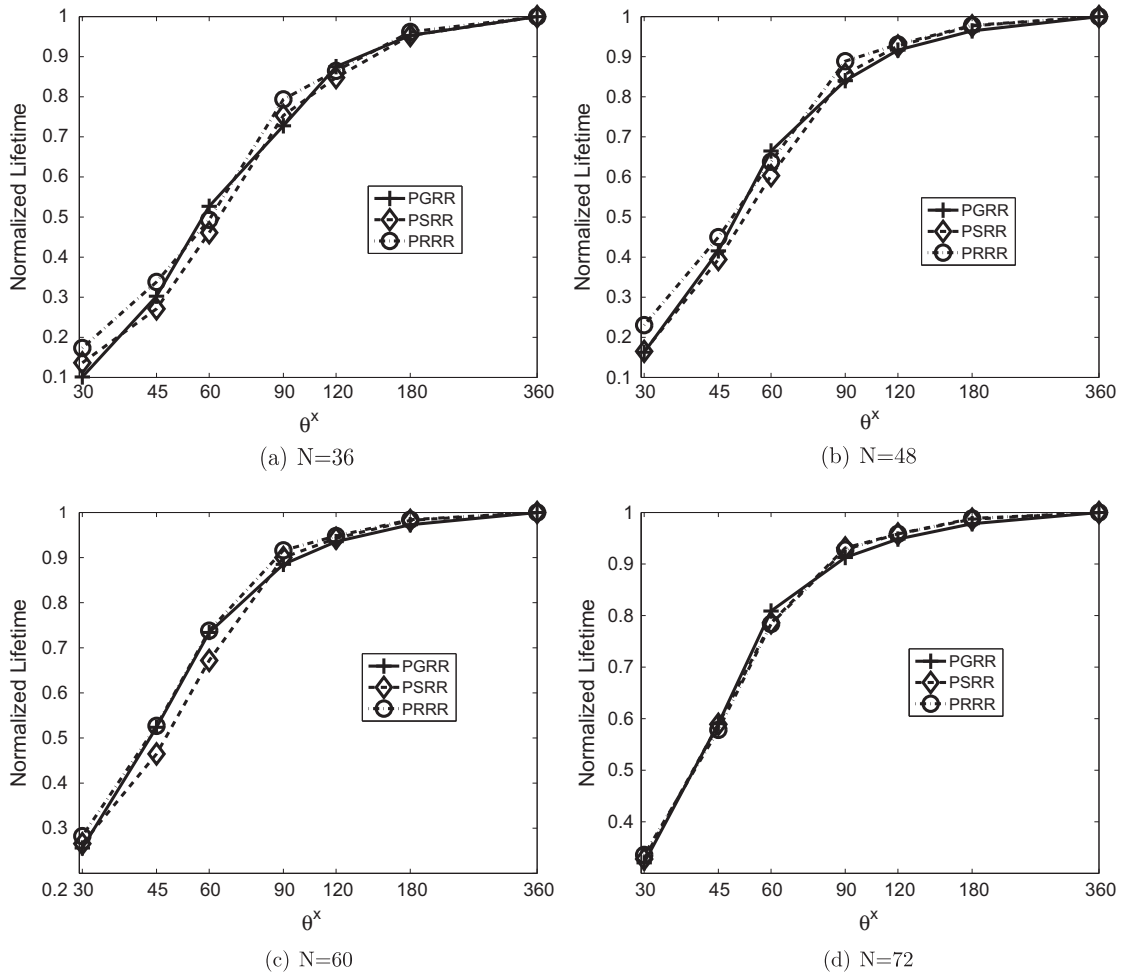

Fig. 7. Normalized lifetime as functions of polar angle (θ^x). Data points presented in the figure are the averages of 500 independent runs.

increasing polar angle despite the fact that N is kept constant. The reason for such behavior is that by increasing the polar angle the number of problems to be solved is reduced, yet, the problem size is increased. For example, with $\theta^{PGRR} = 45$ and $N = 48$, there are four routing domains with 12 sensor nodes, whereas, with $\theta^{PGRR} = 360$ and $N = 48$, there is a single routing domain with 48 sensor nodes. Solving four MIP problems with 12 sensor node domains takes much lower time than solving a single MIP problem with 48 sensor nodes. Different regimes do not have a decisive advantage against each other in terms of solution times. Nevertheless, the dominant factor in the solution times is N.

5. Discussion

In this study, we do not propose a new MAC or routing protocol to maximize WSN lifetime. Instead, we analyze the routing localization–scalability from network lifetime maximization perspective within a general framework and without going into the details of specific routing protocols or algorithms. In fact, MIP based optimization of data flows in the network to maximize the lifetime is an abstraction for an idealized WSN routing protocol. By doing so we eliminate the possible suboptimal behaviors of routing protocols' implementation details not specifically related to the concept under investigation, *per se*. Nevertheless, the results of this study can be used as guidelines in designing distributed algorithms. For example, one of the design guidelines we identified is that without sacrificing from the maximum achievable lifetime, it is not possible to achieve any level of localization. This fact will hold for any well designed WSN routing protocol. Therefore, a comparison of the results of the MIP framework against any WSN protocol is not meaningful in this context. If we were to design a distributed protocol architecture then a comparison against existing WSN protocol architectures would be necessary. Furthermore, the performance benchmarks uncovered by the MIP framework presented in this study would serve as an upper limit for the performance of such distributed protocol architectures. However, the design of a distributed protocol architecture is beyond the scope of our study.

In our framework we assume that a TDMA-based MAC layer is in operation which mitigates interference between

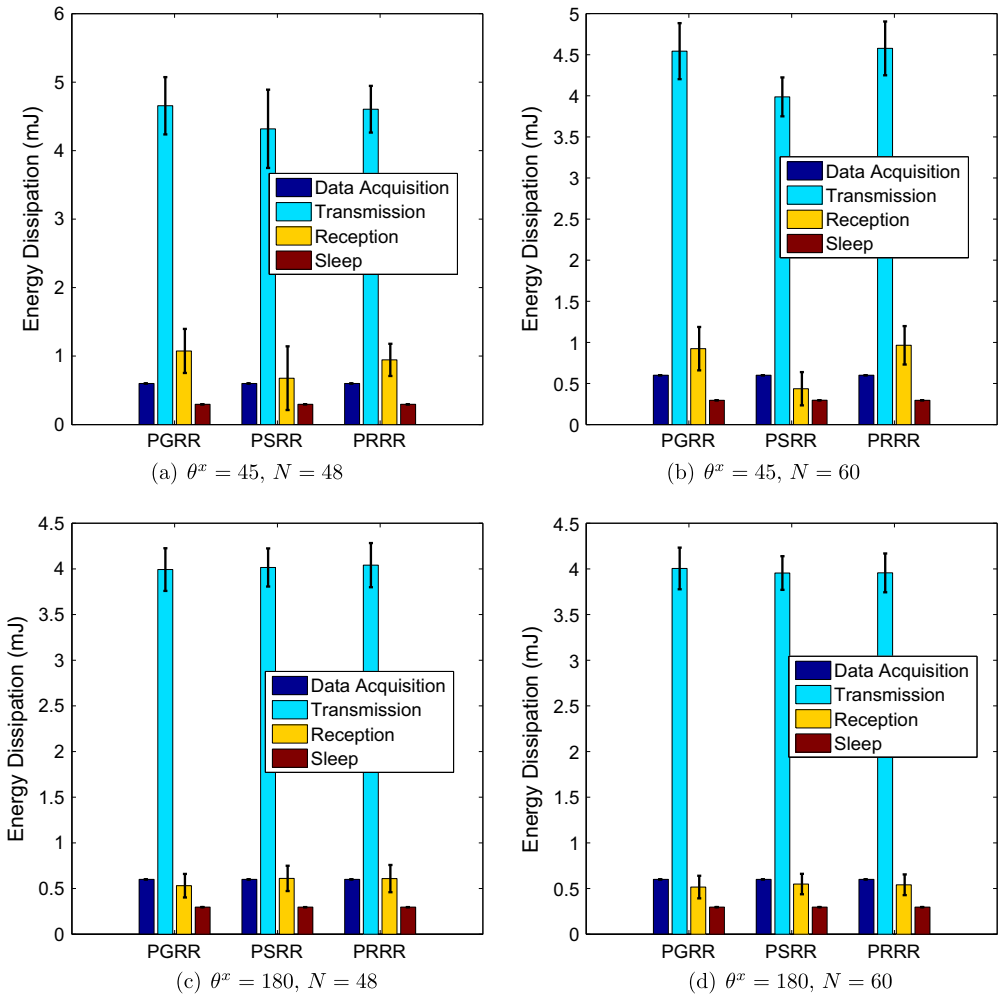

Fig. 8. Detailed energy dissipation results for various θ^x and N values. Energy dissipation values are normalized with the number of nodes and the total network lifetime (in terms of rounds), thus, the energy values are in terms of per node per round. Data points presented in the figure are the averages of 500 independent runs.

Table 4
Time complexity of the MIP model in terms of seconds. In $x \pm y$ notation, x and y denote the average and the standard deviation, respectively.

	$N = 36$	$N = 48$	$N = 60$	$N = 72$
$\theta^{PGRR} = 45$	1.40 ± 0.19	3.32 ± 0.49	7.60 ± 1.30	15.03 ± 11.76
$\theta^{PGRR} = 90$	2.10 ± 1.18	5.55 ± 1.12	12.87 ± 3.11	37.59 ± 21.15
$\theta^{PGRR} = 180$	5.25 ± 1.87	17.68 ± 5.81	50.45 ± 11.72	197.92 ± 57.25
$\theta^{PGRR} = 360$	21.94 ± 13.50	67.19 ± 15.01	237.20 ± 38.45	757.22 ± 127.50
$\theta^{PSRR} = 45$	1.11 ± 0.11	2.23 ± 0.25	4.58 ± 0.53	9.20 ± 0.66
$\theta^{PSRR} = 90$	1.12 ± 0.10	2.24 ± 0.17	5.93 ± 2.01	11.70 ± 2.38
$\theta^{PSRR} = 180$	2.67 ± 1.57	17.11 ± 8.22	49.58 ± 6.46	195.35 ± 53.00
$\theta^{PSRR} = 360$	15.92 ± 6.39	78.54 ± 17.29	248.85 ± 31.14	1296.83 ± 140.16
$\theta^{PRRR} = 45$	1.34 ± 0.14	2.32 ± 0.20	4.75 ± 0.90	10.04 ± 1.00
$\theta^{PRRR} = 90$	2.02 ± 0.77	6.53 ± 2.22	18.34 ± 4.77	84.28 ± 7.22
$\theta^{PRRR} = 180$	6.99 ± 3.26	38.51 ± 3.62	74.99 ± 9.13	463.22 ± 29.07
$\theta^{PRRR} = 360$	19.04 ± 5.66	83.01 ± 25.20	367.86 ± 44.29	1479.76 ± 213.20

active links through a time-slot assignment algorithm which outputs a conflict-free transmission schedule. A combinatorial interference model can be used to model interference [35,36]. In [30,31], it is shown that such an algorithm is possible hence collision free communication is achieved if bandwidth requirements are satisfied. In fact,

in our model, we use a modified version of the sufficient condition presented in [30,31]. Furthermore, it is also possible to reduce data packet collisions to negligible levels in practical MAC protocols designed with a dynamic TDMA approach [37,38]. It is also shown that well designed Carrier Sense Multiple Access (CSMA) based MAC protocols are highly successful in reducing the collision rate to negligible levels provided that the network traffic is much lower than the available capacity [39–41]. Note that in the numerical analysis, we choose the parameters affecting Eq. (19) in such a way that the maximum value of the left hand side of the inequality is more than an order of magnitude lower than the right hand side value.

We do not have a constraint on the buffer capacity of the sensor nodes in our framework. Therefore, the packet buffer size is, conceptually, unlimited. However, the actual maximum packet buffer size is limited by the number of sensor nodes in the networks because each sensor node generates one data packet per round and each generated data packet can reach the base station within the round it is generated.

Note that the current and voltage characteristics of batteries deviate from the nominal values throughout the lifetime of the batteries, especially, when the batteries approach total discharge. Thus, the sensor nodes running on such batteries can perform suboptimally as the battery characteristics deteriorate. However, in our system model we ignore such properties of practical batteries.

6. Conclusion

In the long term, smart grid will be the ultimate destination for electric power systems. Wireless ad hoc architecture will play a key role in the communication infrastructure of smart grid systems. In wide-area network deployments, scalability of routing protocols geared towards the needs of many-to-one sensors-to-sink communication is an important topic of interest. Traditionally, the problem of scalability could be tackled with localized routing. However, the lack of global information exchange would lead to suboptimal routing paths and thus have a negative impact on network lifetime, which is a serious concern for WSNs.

In this paper, we presented a novel MIP framework that models both the energy dissipation characteristics of WSNs and flow optimization for energy balancing. Using this framework we investigated the tradeoff between network lifetime maximization and flow localization for scalability using three localized routing regimes.

Our study closes the gap between two important performance metrics in smart grid communication networks (routing localization–scalability and network lifetime) through the developed framework. The numerical results show that it is not possible to achieve any level of localization without sacrificing from the maximum achievable network lifetime. However, if lifetime decrease to a certain extent can be tolerated, localization is a viable option (*e.g.*, the decrease in network lifetime using Per Relay Routing Regime with $\theta^{PRRR} = 180, \theta^{PRRR} = 120$, and $\theta^{PRRR} = 90$ can be as low as 1%, 4%, and 7%, respectively).

References

[1] B. Liscouski, W. Elliot, Final report on the august 14, 2003, blackout in the united states and canada: causes and recommendations, Tech. Rep., U.S. Department of Energy, 2004.

[2] C.W. Johnson, Analysing the causes of the Italian and Swiss blackout, 28 th september 2003, in: Proc. Australian Workshop on Safety Critical Systems and Software and Safety-Related Programmable Systems (SCS), vol. 86, 2007, pp. 21–30.

[3] N. Saputro, K. Akkaya, S. Uludag, A survey of routing protocols for smart grid communications, Comput. Netw. 56 (2012) 2742–2771.

[4] M. Erol-Kantarci, H.T. Mouftah, Wireless multimedia sensor and actor networks for the next generation power grid, Ad Hoc Netw. 9 (2011) 542–551.

[5] R.A. León, V. Vittal, G. Manimaran, Application of sensor network for secure electric energy infrastructure, IEEE Trans. Power Deliv. 22 (2007) 1021–1028.

[6] Grid 2030: A National Vision for Electricity's Second 100 Years, Tech. Rep., U.S. Department of Energy, 2003.

[7] Towards Smart Power Networks: Lessons Learned from European Research FP5 Projects, Tech. Rep., European Commision, 2005.

[8] Epri Intelligrid, 2008. <http://intelligrid.epri.com>.

[9] P. Zhang, F. Li, N. Bhatt, Next-generation monitoring, analysis, and control for the future smart control center, IEEE Trans. Smart Grid 1 (2010) 186–192.

[10] Y.J. Kim, J. Lee, G. Atkinson, H. Kim, M. Thottan, Sedax: a scalable, resilient, and secure platform for smart grid communications, IEEE J. Sel. Area. Commun. 30 (2012) 1119–1136.

[11] V.C. Gungor, B. Lu, G.P. Hancke, Opportunities and challenges of wireless sensor networks in smart grid, IEEE Trans. Ind. Electron. 57 (2010) 3557–3564.

[12] Y. Yang, F. Lambert, D. Divan, A survey on technologies for implementing sensor networks for power delivery systems, in: Proc. IEEE Power Engineering Society General Meeting (PES GM), 2007, pp. 1–8.

[13] I.F. Akyildiz, W. Su, Y. Sankarasubramaniam, E. Cayirci, Wireless sensor networks: a survey, Comput. Netw. 38 (2002) 393–422.

[14] E. Hossain, Z. Han, H.V. Poor, Smart Grid Communications and Networking, Cambridge University Press, 2012.

[15] Industrial Wireless Technology for 21st Century, Tech. Rep., U.S. Department of Energy, 2002.

[16] L.L. Peterson, B.S. Davie, Computer Networks – A Systems Approach, 3rd ed., Morgan Kaufmann, 2003. ISBN 978-1-55860-832-0.

[17] Z. Cheng, M. Perillo, W. Heinzelman, General network lifetime and cost models for evaluating sensor network deployment strategies, IEEE Trans. Mobile Comput. 7 (2008) 484–497.

[18] Y. Wang, X.Y. Li, W.Z. Song, M. Huang, T.A. Dahlberg, Energy-efficient localized routing in random multihop wireless networks, IEEE Trans. Parallel Distr. Syst. 22 (2011) 1249–1257.

[19] L. Wolsey, Integer Programming, Wiley Interscience Publication, 1998.

[20] F. Ishmanov, A.S. Malik, S.M. Kim, Energy consumption balancing (ECB) issues and mechanisms in wireless sensor networks (WSNs): a comprehensive overview, Euro. Trans. Telecommun. 22 (2011) 151–167.

[21] A. Gogu, D. Nace, A. Dilo, N. Meratnia, Review of optimization problems in wireless sensor networks, in: J. Hamilton Ortiz (Ed.), Telecommunications Networks – Current Status and Future Trends, InTech, 2012, pp. 153–180.

[22] G. Anastasi, M. Conti, A. Falchi, E. Gregori, A. Passarella, Performance measurements of motes sensor networks, in: Proc. ACM International Symposium on Modeling, Analysis and Simulation of Wireless and Mobile Systems (MSWiM), 2004, pp. 174–181.

[23] M. Schuts, F. Zhu, F. Heidarian, F.W. Vaandrager, Modelling clock synchronization in the Chess gMAC WSN protocol, in: Proc. Workshop on Quantitative Formal Methods: Theory and Applications (QFM), vol. 13, 2009, pp. 41–54.

[24] B. Sundararaman, U. Buy, A.D. Kshemkalyani, Clock synchronization for wireless sensor networks: a survey, Ad Hoc Netw. 3 (2005) 7281–7323.

[25] S. Ganeriwal, R. Kumar, M.B. Srivastava, Timing-sync protocol for sensor networks, in: Proc. ACM Conference on Embedded Networked Sensor Systems (SenSys), 2003, pp. 138–149.

[26] K. Bilinska, M. Filo, R. Krystowski, Mica, Mica2, MicaZ, 2007. <http://wwwpub.zih.tu-dresden.de/~dargie/wsn/slides/students/MICA.ppt>.

[27] M. Saxena, P. Gupta, B.N. Jain, Experimental analysis of rssi-based location estimation in wireless sensor networks, in: Proc.

International Conference on Communication Systems Software and Middleware and Workshops (COMSWARE), 2008, pp. 503–510.
[28] J. Vales-Alonso, E. Egea-Lopez, A. Martinez-Sala, P. Pavon-Marino, M.V. Bueno-Delgado, J. Garcia-Haro, Performance evaluation of MAC transmission power control in wireless sensor networks, Comput. Netw. 51 (2007) 1483–1498.
[29] M. Rahimi, R. Baer, O. Iroezi, J. Garcia, J. Warrior, D. Estrin, et al., Cyclops: in situ image sensing and interpretation in wireless sensor networks, in: Proc. ACM Conference on Embedded Networked Sensor Systems (SenSys), 2005, pp. 192–204.
[30] M. Cheng, X. Gong, L. Cai, Joint routing and link rate allocation under bandwidth and energy constraints in sensor networks, IEEE Trans. Wireless Commun. 8 (2009) 3770–3779.
[31] H. Cotuk, B. Tavli, K. Bicakci, M.B. Akgun, The impact of bandwidth constraints on the energy consumption of wireless sensor networks, in: Proceedings of the IEEE Wireless Communication and Networking Conference (WCNC), 2014.
[32] D.F. Macedo, L.H.A. Correia, A.L. dos Santos, A.A.F. Loureiro, J.M.S. Nogueira, G. Pujolle, A Comprehensive Evaluation of Transmission Power Control on Mobile Ad hoc Networks, Tech. Rep. RT.DCC.003, Computer Science Department of the Federal University of Minas Gerais, Belo Horizonte, MG, Brazil, 2008.
[33] L. Ma, B. Li, Z.B. Yang, J. Du, J. Wang, A new combination prediction model for short-term wind farm output power based on meteorological data collected by wsn, Int. J. Control Autom. 7 (2014) 171–180.
[34] General Algebraic Modeling System (GAMS), 2013. <http://www.gams.com/>.
[35] K. Jain, J. Padhye, V.N. Padmanabhan, L. Qiu, Impact of interference on multi-hop wireless network performance, in: Proc. ACM Annual International Conference on Mobile Computing and Networking (MOBICOM), 2003, pp. 66–80.
[36] P. Gupta, P.R. Kumar, The capacity of wireless networks, IEEE Trans. Inform. Theory 46 (2000) 388–404.
[37] I. Demirkol, C. Ersoy, F. Alagoz, MAC protocols for wireless sensor networks: a survey, IEEE Commun. Mag. 44 (2006) 115–121.
[38] B. Tavli, W. Heinzelman, Energy and spatial reuse efficient network-wide real-time data broadcasting in mobile ad hoc networks, IEEE Trans. Mobile Comput. 5 (2006) 1297–1312.
[39] M. Miskowicz, M. Sapor, M. Zych, W. Latawiec, Performance analysis of predictive p-persistent CSMA protocol for control networks, in: Proc. IEEE International Workshop on Factory Communication Systems (WFCS), 2002, pp. 249–256.
[40] K. Duffy, D. Malone, D. Leith, Modeling the 802.11 distributed coordination function in non-saturated conditions, IEEE Commun. Lett. 9 (2005) 715–717.
[41] D. Malone, K. Duffy, D. Leith, Modeling the 802.11 distributed coordination function in nonsaturated heterogeneous conditions, IEEE/ACM Trans. Network. 15 (2007) 159–172.

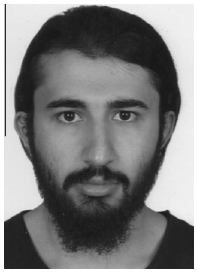

Erkam Uzun is currently an M.Sc. student at the Computer Engineering Department, TOBB University of Economics and Technology, Ankara, Turkey. He received the B.Sc. degrees in both Computer Engineering and Electrical & Electronics Engineering in 2011 from TOBB University of Economics and Technology, Ankara, Turkey. Telecommunications, digital forensics, multimedia computing and security are his current research areas.

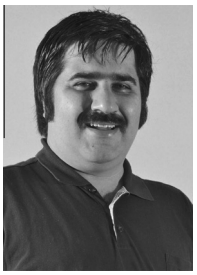

Bulent Tavli is currently an associate professor at the Department of Electrical and Electronics Engineering, TOBB University of Economics and Technology, Ankara, Turkey. He received the B.S. degree in Electrical and Electronics Engineering in 1996 from the Middle East Technical University, Ankara, Turkey. He received the M.S. and Ph.D. degrees in Electrical and Computer Engineering in 2001 and 2005 from the University of Rochester, Rochester, NY, USA. Telecommunications, networking, mathematical programming, signal processing, and embedded systems are his current research areas.

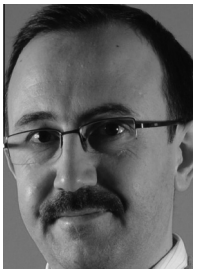

Kemal Bicakci is currently an associate professor at the Computer Engineering Department, TOBB University of Economics and Technology, Ankara, Turkey. He has obtained his Ph.D. degree from Middle East Technical University, Ankara, Turkey in 2003. His research interests include wireless and sensor networks, information security, applied cryptography, and usability.

Davut Incebacak is currently a Ph.D. student at the Informatics Institute, Middle East Technical University, Ankara, Turkey. He has obtained his M.Sc. degree in 2007 from the Informatics Institute, Middle East Technical University, Ankara, Turkey. He received the B.Sc. degrees in Computer Engineering in 2002 from Sakarya University, Sakarya, Turkey. His research interests include wireless networks, optimization, and information security.